Insights into the Cellular Response Triggered by Silver Nanoparticles Using Quantitative Proteomics

Thiago Verano-Braga,[†] Rona Miethling-Graff,[‡] Katarzyna Wojdyla,[†] Adelina Rogowska-Wrzesinska,[†] Jonathan R. Brewer,[§] Helmut Erdmann,[‡] and Frank Kjeldsen[†,*]

[†]Protein Research Group and [§]MEMPHYS Center for Biomembrane Physics, Department of Biochemistry and Molecular Biology, University of Southern Denmark, Odense, DK-5230, Denmark and [‡]Biotechnology, University of Applied Science, Flensburg D-24905, Germany

ABSTRACT The use of nanoparticles in foods, materials, and clinical treatments has increased dramatically in the past decade. Because of the possibility of human exposure to nanoparticles, there is an urgent need to investigate the molecular mechanisms underlying the cellular responses that might be triggered. Such information is necessary to assess potential health risks arising from the use of nanoparticles, and for developing new formulations of next generation nanoparticles for clinical treatments. Using mass spectrometry-based proteomic technologies and complementary techniques (*e.g.*, Western blotting and confocal laser scanning microscopy), we present insights into the silver nanoparticle—protein interaction in the human LoVo cell line. Our data indicate that some unique cellular processes are driven by the size. The 100 nm nanoparticles exerted indirect effects *via* serine/threonine protein kinase (PAK), mitogen-activated protein kinase (MAPK), and phosphatase 2A pathways, and the 20 nm nanoparticles induced direct effects on cellular stress, including generation of reactive oxygen species and protein carbonylation. In addition, we report that proteins involved in SUMOylation were up-regulated after exposure to 20 nm silver nanoparticles. These results were further substantiated by the observation of silver nanoparticles entering the cells; however, data indicate that this was determined by the size of the nanoparticles, since 20 nm particles entered the cells while 100 nm particles did not.

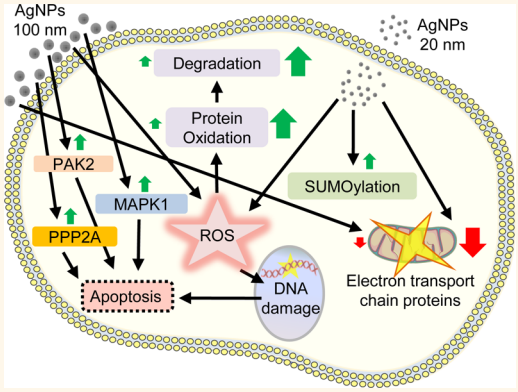

KEYWORDS: iTRAQ · silver nanoparticles · proteomics · cytotoxicity · mass spectrometry · sumoylation · ubiquitination

Silver nanoparticles (AgNPs) are broad spectrum antimicrobial agents with proven activity against multidrug-resistant bacteria, fungi, and viruses, including HIV and SARS.[1,2] Therefore, AgNPs-based products are a growing market that includes wound dressings, athletic socks, toothpaste, mouthwash, food storage bags, and even dietary supplements.[3] It is important to learn whether human exposure to AgNPs is harmful, and the nature of any molecular mechanisms that might underlie nanoparticle—biological (nano—bio) interactions.

Publications using *in vitro* and *in vivo* models report that AgNPs induce toxicity in a manner that depends upon both dosage and particle size. For instance, oral administration of 60 nm AgNPs (30—1000 mg/(kg day)) to rats for 28 or 90 days led to a dose-dependent silver accumulation in the brain, blood, kidneys, lungs, stomach, testes, but primarily the liver, where AgNPs induced dilatation of the central vein and bile-duct hyperplasia.[4,5] A gender specific silver accumulation in the kidneys was found; female rats showed high levels of AgNPs in all kidney regions, especially in the glomerulus.[5] From a toxicological point of view, smaller particle sizes and hence greater surface areas tend to induce higher cytotoxicity when compared to larger particle sizes. For example, Carlson *et al.*[6] reported that AgNPs exposure induced a size-dependent reactive oxygen species (ROS) generation and Kim and colleagues[7] observed that 10 nm AgNPs induced more apoptotic cells than the larger particles (*i.e.*, 50 and 100 nm).

In vitro studies report that the cytotoxicity induced by AgNPs involves production of ROS, cell cycle arrest, and genotoxicity, which leads to inflammation, apoptosis, and cell death.[8,9] Using an *in vitro* model for the human intestinal epithelium and

* Address correspondence to frankk@bmb.sdu.dk.

Received for review September 30, 2013 and accepted February 10, 2014.

Published online February 10, 2014
10.1021/nn4050744

transcriptomic analysis, Bouwmeester *et al.*[10] reported that AgNPs ranging from 20 to 110 nm crossed the *in vitro* intestinal barrier and induced changes in the amounts of mRNAs involved in oxidative stress, endoplasmic reticulum stress response, and apoptosis. Since treatment with silver nitrate ($AgNO_3$) induced regulation of the same set of genes, and 6−17% of the silver content in the AgNPs suspensions was found in the ionic form (Ag^+), the authors speculated that the observed gene regulation was exerted by Ag^+ released from the AgNPs. Recently, Singh and Ramarao[9] reported that after macrophages engulfed 43.9 nm AgNPs by way of the scavenger receptor (SR), the AgNPs released Ag^+ inside the cells, which interfered with mitochondrial activity and induced apoptosis. Thus, cytotoxicity induced by AgNPs is a complex mechanism and intra- and/or extra- cellular effects triggered by nanoparticles must be distinguished from those of the Ag^+ released from the nanoparticles.

State-of-the-art imaging techniques (*e.g.*, confocal microscopy and single-particle tracking microscopy) have been employed to successfully study the cellular uptake, trafficking, and processing of nanoparticles, which improved understanding of nano−bio interactions. Such approaches do not yield information about protein−protein interactions, whereas mass spectrometry (MS)-based proteomics can be a useful tool since it can be used to accurately identify and quantify proteins involved in cellular events underlying nano−bio interactions.[11]

MS-based proteomics in combination with complementary analytical techniques is rarely applied to the analysis of cellular responses to nanoparticles. Preferably, comprehensive analysis requires the use of the exceptionally sensitive modern mass spectrometric instrumentation. Thus, the present work aimed at unraveling the set of proteins and cellular networks that are regulated by AgNPs. Because AgNPs are being used extensively by the food industry, we decided to use human colon carcinoma cell line (LoVo) as an *in vitro* model of the human intestinal tract to evaluate the possible AgNPs toxicity. LoVo cells were exposed with well characterized AgNPs (20 and 100 nm particles), and protein abundances were monitored by tandem MS (MS/MS). Cellular oxidative stress induced by the AgNPs was monitored *in vitro* by measuring ROS generation, and global protein carbonylation was quantified with Western blots. Finally, cellular uptake of the nanoparticles was evaluated by confocal laser scanning microscopy (CLSM).

RESULTS AND DISCUSSION

Characterization of Silver Nanoparticles. Sizes of spherical citrate stabilized AgNPs provided by the manufacturer based on transmission electron microscopy (TEM) were 19.2 ± 2.2 and 99.4 ±7.0 nm. In-house dynamic light scattering (DLS) experiments gave 20.6 ±1.7 and 93.1 ±3.8 nm, respectively (Figure 1). Table 1 summarizes the nanoparticle sizes and ζ-potentials provided by the manufacturer and the values measured in our DLS analysis.

The behavior of citrate-stabilized AgNPs in RPMI 1640 cell culture medium supplemented with 10% fetal calf serum (FCS) has already been studied using dynamic light scattering (DLS) analysis. The nanoparticles were monitored for 24 h and remained well disperse with no aggregation.[12,13]

Proteomics Experimental Conditions. MS-based shotgun proteomics was employed to study the differential regulation of proteins triggered by AgNPs. LoVo cells were exposed to 10 μg/mL AgNPs for 24 h. After preparation of a cell lysate, proteins were digested with trypsin and peptides were labeled with iTRAQ and quantified by MS/MS using untreated cells as the experimental control (Figure 2) (see ref 14 for detailed information about mass spectrometry-based peptide quantification using iTRAQ).

To address whether the cellular responses triggered by AgNPs exposure were size dependent, 20 and 100 nm particles were tested separately in this study. Under oxidative conditions in solution, AgNPs release silver ions (Ag^+), which are known to be toxic to human cells.[15] Therefore, to address whether the amount of Ag^+ present in the culture medium would induce changes in the LoVo proteome, we included nanoparticle-free controls containing any Ag^+ released from the AgNPs. Briefly, the culture medium was incubated with AgNPs for 24 h and centrifuged, and the supernatant free of nanoparticles was collected and used to expose the cells. In this study, the terms Ctrl 20 nm and Ctrl 100 nm (Ctrl stands for "control") were used to define the supernatant collected from media incubated with 20 and 100 nm AgNPs, respectively.

Two-dimensional chromatography is often used in proteomics to increase peptide identification by reducing sample complexity. Since hydrophilic interaction liquid chromatography (HILIC) and reversed-phase chromatography (RP) have a high degree of orthogonality,[16] we prefractionated the samples off-line with HILIC before online RP-LC−MS/MS analysis (Figure 2). In addition to sample complexity, peptide supercharging induced by iTRAQ reagents (especially for 8-plex) can compromise peptide identifications.[17] To overcome this problem, we used ammonia evaporation perpendicular to the electrospray needle, which reduces the average charge-state of iTRAQ labeled peptides.[17]

AgNPs Induce Changes in the LoVo Cell Proteome. Using the experimental strategy depicted in Figure 2, 3352 protein groups (Supporting Information Table 1 and Supporting Information Figure S1) were identified and quantified (at least two high-confidence peptides per protein) and only differentially expressed proteins with p-value ≤ 0.01 were considered to be regulated (Supporting Information Figure S2). Figure 3A depicts

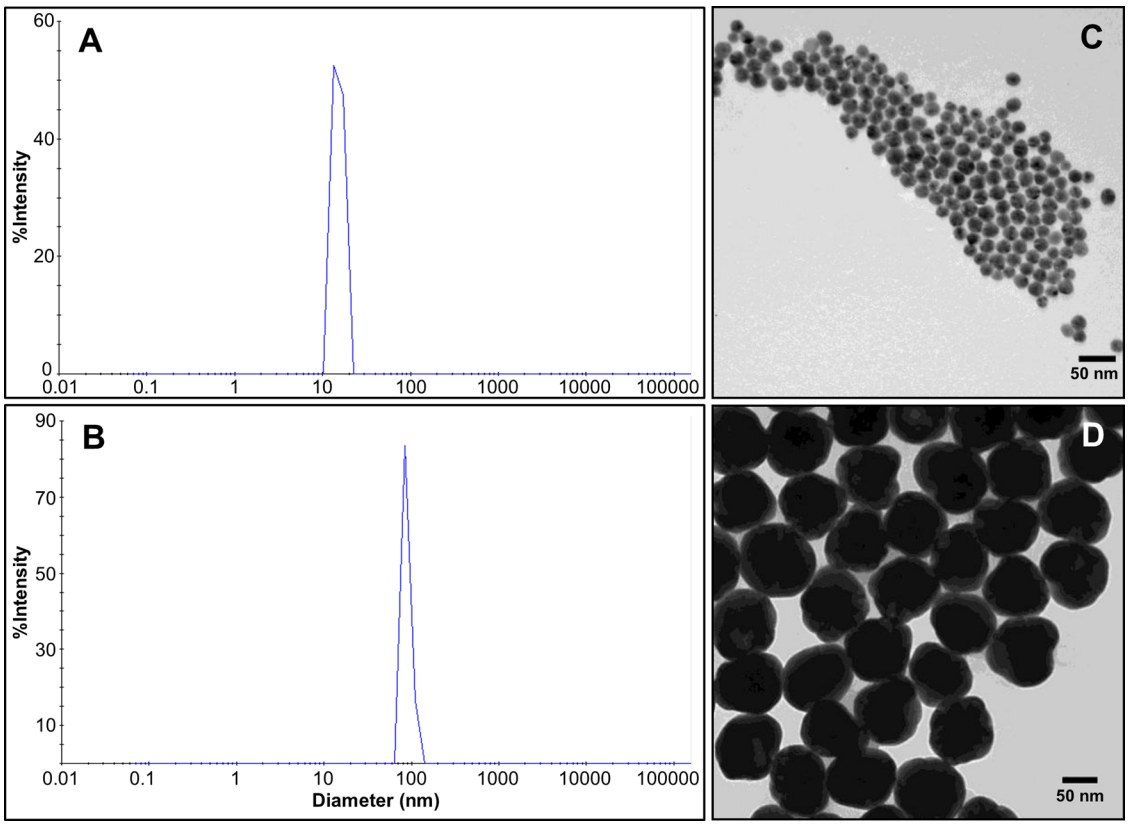

Figure 1. Characterization of the AgNPs sizes. Representative dynamic light scattering (DLS) profiles of 20 nm AgNPs (batch DAC1212) (A) and 100 nm AgNPs (batch DAC1110) (B). Transmission electron microscope (TEM) images provided by the manufacturer from 20 nm AgNPs (C) and 100 nm AgNPs (D).

TABLE 1. Nanoparticles Characterization

sample	diameter (SD)[a] (nm)	ζ-potential (mV)
20 nm AgNPs	20.6 (±1.7)[b]/19.2 (±2.2)[c]	−37.3[b]/−36.8[c]
100 nm AgNPs	93.1 (±3.8)[b]/99.4 (±7.0)[c]	−57.5[b]/−50.6[c]

[a] SD, standard deviation. [b] DLS-based analyses performed in this study. [c] Analyses performed by the manufacturer.

the number of proteins differentially regulated over the four experimental conditions (*i.e.*, 20 nm AgNPs, 100 nm AgNPs, Ctrl 20 nm, and Ctrl 100 nm) relative to the untreated cells. A list of all differentially regulated proteins can be found in Supporting Information Table 2. Six hundred and twenty (620) proteins were differentially regulated by exposure to the 20 nm AgNPs (340 down-regulated and 280 up-regulated), and 717 proteins were regulated by exposure to 100 nm AgNPs (378 down-regulated and 339 up-regulated). Importantly, these results represent proteins regulated by both AgNPs and Ag^+ present in the culture media. Indeed, LoVo cells treated with Ctrl 20 nm and Ctrl 100 nm induced differential regulation of 252 (120 down-regulated and 132 up-regulated) and 458 (254 down-regulated and 204 up-regulated) proteins, respectively (Figure 3A). By removing the proteins that were regulated in the Ctrl 20 nm and Ctrl 100 nm experiments, we identified the proteins that were differentially regulated by only the nanoparticles. Thus, the 20 nm AgNPs induced the specific regulation of 467 proteins (240 down-regulated and 227 up-regulated) and 100 nm AgNPs changed the abundance of 306 proteins (143 down-regulated and 163 up-regulated) (Figure 3B,C, light red color). Only the non-overlapping proteins detected after exposure of 20 nm AgNPs, 100 nm AgNPs, Ctrl 20 nm, and Ctrl 100 nm were included in the further data analysis.

Changes in the LoVo Cell Proteome Due to Nanoparticle Exposure Are Size-Specific. Gene Ontology (GO) analysis was used to gain insight into the biological processes, molecular functions, and cellular localization of the proteins differentially regulated by the AgNPs (20 and 100 nm). The 20 nm nanoparticles (blue bars) induced the regulation of more proteins than the 100 nm particles did (red bars) for all GO terms (Figure 4). Concerning the cellular localization of the regulated proteins, mitochondrial proteins had a tendency to be more down-regulated than up-regulated when exposed to 20 and 100 nm particles. The opposite profile was observed for cytosolic proteins. These data suggest that the AgNPs induced down-regulation of target mitochondrial genes and/or increased protein degradation in mitochondria, while the cytosolic proteins became either more abundant due to increased expression and/or were degraded less efficiently.

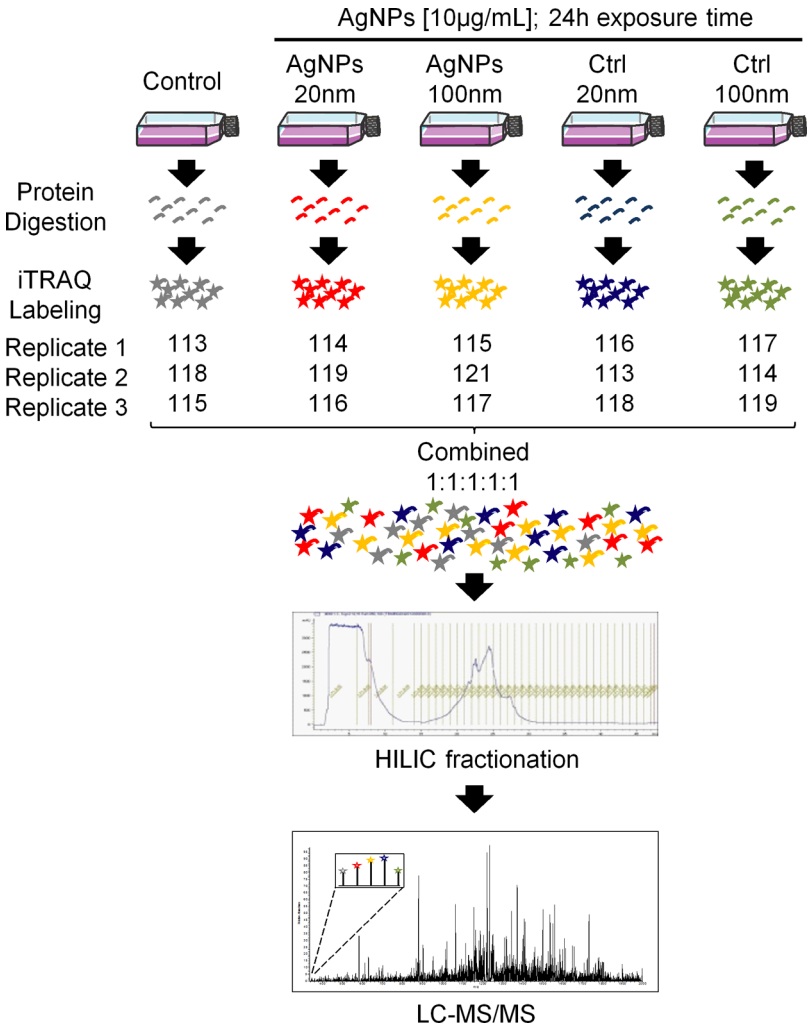

Figure 2. Proteomics experimental conditions. LoVo cells were treated with 20 and 100 nm AgNPs (10 μg) and the Ag^+ ions released from the nanoparticles into the culture media. Untreated cells were used as reference. Proteins were digested with trypsin and labeled with iTRAQ 8-plex. To reduce any label inefficiency of specific iTRAQ tags (*i.e.*, 113, 114, 115, 116, 117, 118, 119 or 121), we did not use the same tag to label the same experimental condition over the three replicates. The samples were combined in equal amounts and subjected to HILIC fractionation. Each of the 10 fractions collected was subjected to LC–MS/MS analysis.

Proteins from proteasome complexes were found up-regulated after the AgNPs treatment, possibly to increase the degradation of proteins damaged by the nanoparticles. In accordance with molecular functions and biological processes of the GO term, up-regulated proteins were associated with antioxidant activity and cell death and down-regulated proteins were involved with cell growth processes. Taken together, these data indicate that the AgNPs (primarily the 20 nm particles) induced changes in the LoVo cells homeostasis, leading to the activation of cellular mechanisms to overcome oxidative stress induced by the nanoparticles.

To better understand the molecular mechanisms underlying the cellular responses triggered by AgNPs, we used the STRING (Search Tool for the Retrieval of Interacting Genes/Proteins) algorithm[18] to build protein–protein interaction networks. Comparisons were made by overlaying these networks with the over-represented biological functions found in the GO analysis (Figure 5 and Supporting Information Figure S3). Figure 5A (20 nm AgNPs) and Figure 5C (100 nm AgNPs) represent the protein–protein interactions of down-regulated proteins, whereas Figure 5B (20 nm AgNPs) and Figure 5D (100 nm AgNPs) depict the interaction networks of the up-regulated ones. Exposure with 20 nm particles resulted in a predominant down-regulation of proteins involved in the mitochondrial electron transport chain (Figure 5A); the same effect was found for 100 nm particles although to a lesser extent (Figure 5C). A cluster containing up-regulated proteins involved in the DNA damage response comprised more interacting proteins after exposure to 20 nm AgNPs (Figure 5B) than 100 nm AgNPs (Figure 5D). The individual proteins involved in the protein–protein clusters of the mitochondrial electron transport chain and DNA damage response are shown in Table 2 and Supporting Information Figure S3. Interestingly, all proteins involved in DNA

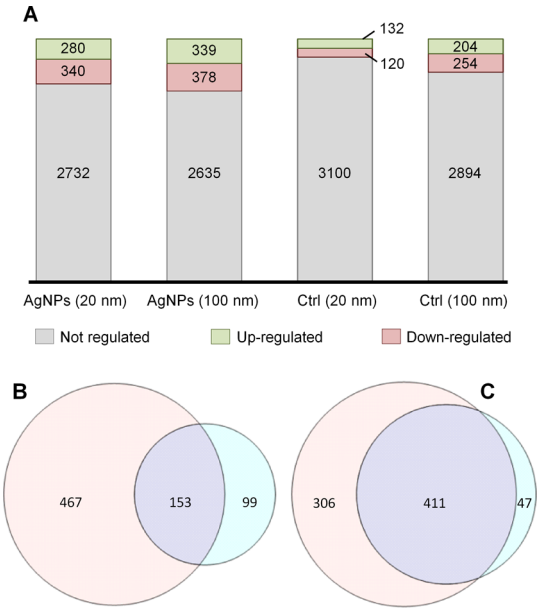

Figure 3. Quantitative proteomics data. (A) In total, 3352 proteins were identified in all four experimental conditions (considering the regulated and not regulated ones). Of these, 620 and 717 proteins were differentially regulated ($p \leq 0.01$) by 20 and 100 nm AgNPs treatment, respectively. Likewise, 252 and 458 proteins were differentially regulated after treatment with the supernatants containing Ag^+ released by 20 nm AgNPs (Ctrl 20 nm) and 100 nm AgNPs (Ctrl 100 nm). (B) Overlap among proteins regulated by 20 nm AgNPs and Ctrl 20 nm supernatant. (C) Overlap among proteins regulated by 100 nm AgNPs and Ctrl 100 nm. To study proteins regulated by the AgNPs only or by Ag^+ only, proteins in nonoverlapping areas were used (light red for AgNPs only and light blue for Ag^+ only).

damage response are components of the proteasome complex, which degrade proteins tagged with ubiquitin as consequence of several cellular processes, including DNA damage.[19]

Two other clusters of interacting proteins observed after exposure of cells to both nanoparticle size included down-regulated proteins involved in the nuclear mRNA splicing *via* spliceosome (Figure 5A,C) and up-regulated proteins involved with the translational initiation process (Figure 5B,D).

Some clusters were observed only after exposure to 20 nm particles: down-regulated proteins involved in mitochondrial translation, RNA processing and cell proliferation (Figure 5A), and the up-regulated proteins involved in the tRNA metabolism (Figure 5B). Concerning the clusters found only upon exposure to 100 nm AgNPs, there were down-regulated proteins related to lipid metabolic processes and protein targeting to membrane (Figure 5C) and up-regulated proteins involved with carbohydrate metabolism and "de novo" protein folding (Figure 5D).

The previous analysis revealed extensive up- and down-regulation caused by AgNPs. Despite the difference in size of the AgNPs, the action of the regulation was similar in affecting proteins involved in the DNA damage response, electron transport chain, and protein translation. However, we wished to determine if the remaining affected proteins differ between the two experiments. To extract this information, we created a hierarchical clustering analysis as illustrated in Figure 6. Proteins with altered abundance because of 20 nm AgNPs exposure were grouped in clusters I (up-regulated) and IV (down-regulated), while proteins differentially regulated by 100 nm particles were grouped in clusters III (up-regulated) and V (down-regulated). Proteins with changes in abundance because of the exposure to both particle sizes were grouped in clusters II (up-regulated) and VI (down-regulated).

Interestingly, the 20 nm AgNPs induced specific up-regulation of the small ubiquitin-related modifier 2 (SUMO2, cluster I). SUMOylation is a post-translational modification of target proteins catalyzed by three enzymes (E1, E2, and E3) that is triggered by several cellular events such as protein instability, DNA damage, generation of ROS, and apoptosis. TRIM28, a protein with E3 activity,[20] was also positively regulated by 20 nm AgNPs, suggesting that SUMO pathway is activated when the LoVo cells are exposed to the smaller particle size. The effect of SUMOylation is still a matter of debate, although studies have shown that protein SUMOylation mediates subcellular protein localization, regulation of target protein function and stabilization. In addition, reports have shown that SUMOylation for some proteins counteract the function of ubiquitination that otherwise induces protein degradation.[21] From the data at hand, it is not possible to determine the exact SUMO target proteins of LoVo cells and further investigations are needed to elucidate these pathways.

Among the proteins specifically regulated by 100 nm particles, protein kinases MAPK1 and PAK2 were up-regulated (cluster III), suggesting that exposure to 100 AgNPs activated the signaling cascades mediated by these kinases. PAK2 and MAPK1 mediate apoptosis in a caspase-dependent[22] and caspase-independent manner,[23] respectively. Our results are in line with previous observations that AgNPs but not Ag^+ induced DNA damage and apoptosis in Jurkat T Cells by way of MAPK activation.[24] The catalytic (PPP2CA) and regulatory (PPP2R1A) subunits of the phosphatase 2A were also up-regulated when exposed to 100 nm AgNPs, which is consistent with a negative control of cell growth and division and a positive control of apoptosis.[25]

Finally, several proteins from the proteasome and ribosome complexes and proteins associated with ubiquitination were up-regulated after exposure to 20 and 100 nm AgNPs (cluster II), suggesting that nanoparticles induced protein damage that were targeted to degradation by way of the ubiquitin–proteasome system and new proteins were synthesized

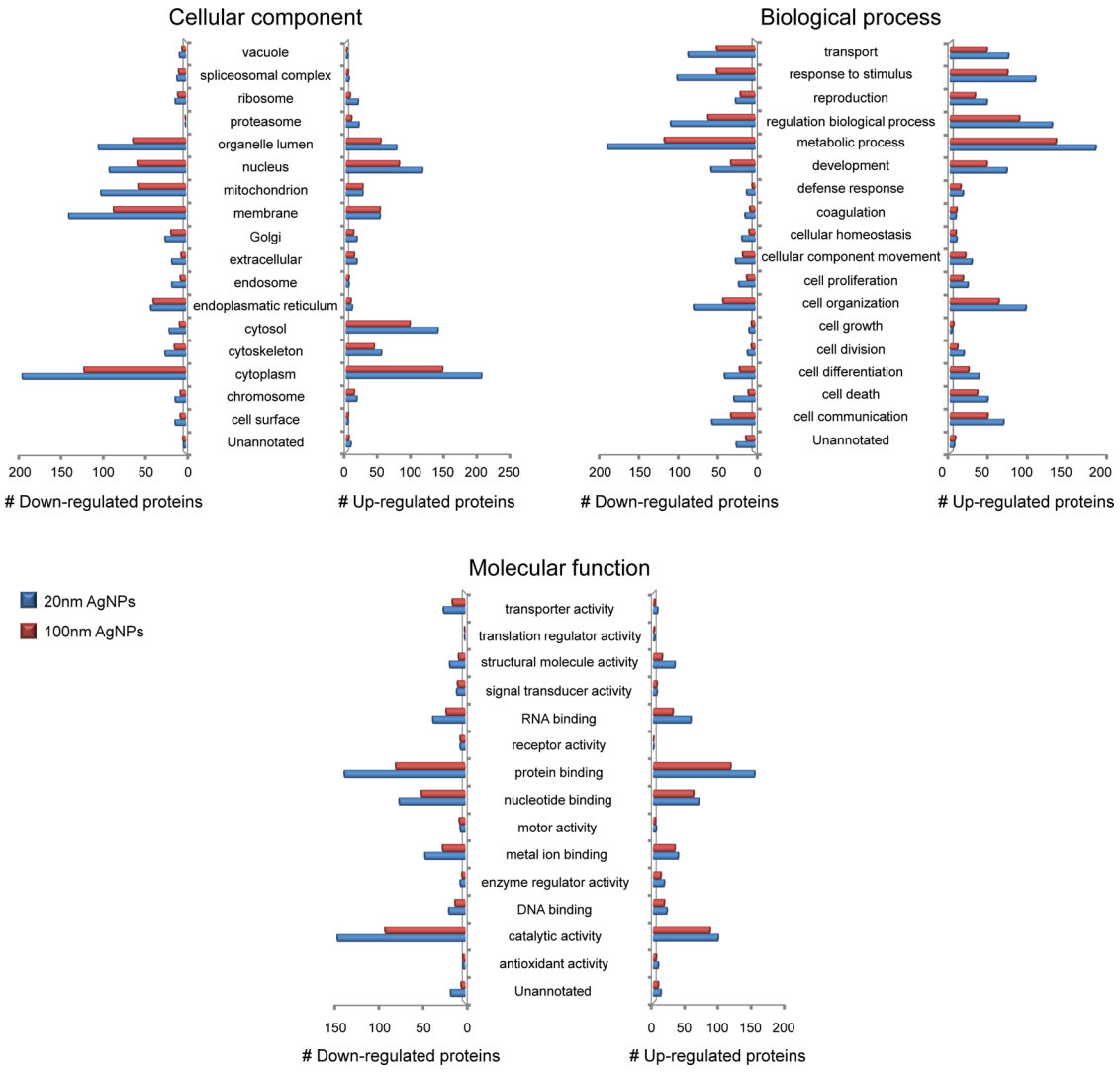

Figure 4. Gene Ontology analysis. Only differentially regulated proteins were subject to Gene Ontology (GO) analysis. These pictures show the up- and down-regulated GO terms for cellular compartments, molecular functions, and biological processes of the proteins. The blue bars represent proteins regulated by 20 nm AgNPs and the red bars represent proteins regulated by 100 nm AgNPs.

to replace them. Ubiquitination seems to play an important role during the exposure of human cells to nanoparticles in general. Recently, Yan and collaborators[26] reported that following the cellular internalization of nanoporous polymer particles (NPPs), which is a system that can be used as drugs delivery, regulation events of proteins related to the ubiquitin network were observed.

Taken together, the proteomics data suggest that exposure to 20 nm AgNPs and to a lesser extent 100 nm AgNPs induces cellular oxidative stress leading to (i) DNA damage and apoptosis, (ii) protein damage leading to ubiquitination and degradation by way of proteasomes, and (iii) reduction in mitochondrial activity as an outcome of down-regulation of proteins involved with the electron transport chain.

Evaluation of the Oxidative Stress Induced by AgNPs Using *in Vitro* Assays. Since the proteomic data showed that primarily 20 nm AgNPs induced up-regulation of proteasome and ubiquitin-related proteins, we speculated that protein degradation pathways were activated. These events can be a consequence of extensive protein carbonylation caused by an increase in the cytosolic ROS. To test this hypothesis, we performed a Western blot assay specific for protein carbonylation (OxyBlot) and measured the intracellular ROS levels using the fluorescent marker H_2DCF-DA (Figure 7).

Figure 7A–C depicts the detection and quantification of global protein carbonylation in LoVo cells exposed with 10 μg/mL (20 or 100 nm) AgNPs for 24 h. Only cells exposed to 20 nm AgNPs resulted in measurable protein carbonylation (Figure 7A,C). A protein loading control ensured that the amount of protein loaded onto the gel was equal under all conditions (Figure 7B). These results are in line with a previous study reporting increased protein carbonylation

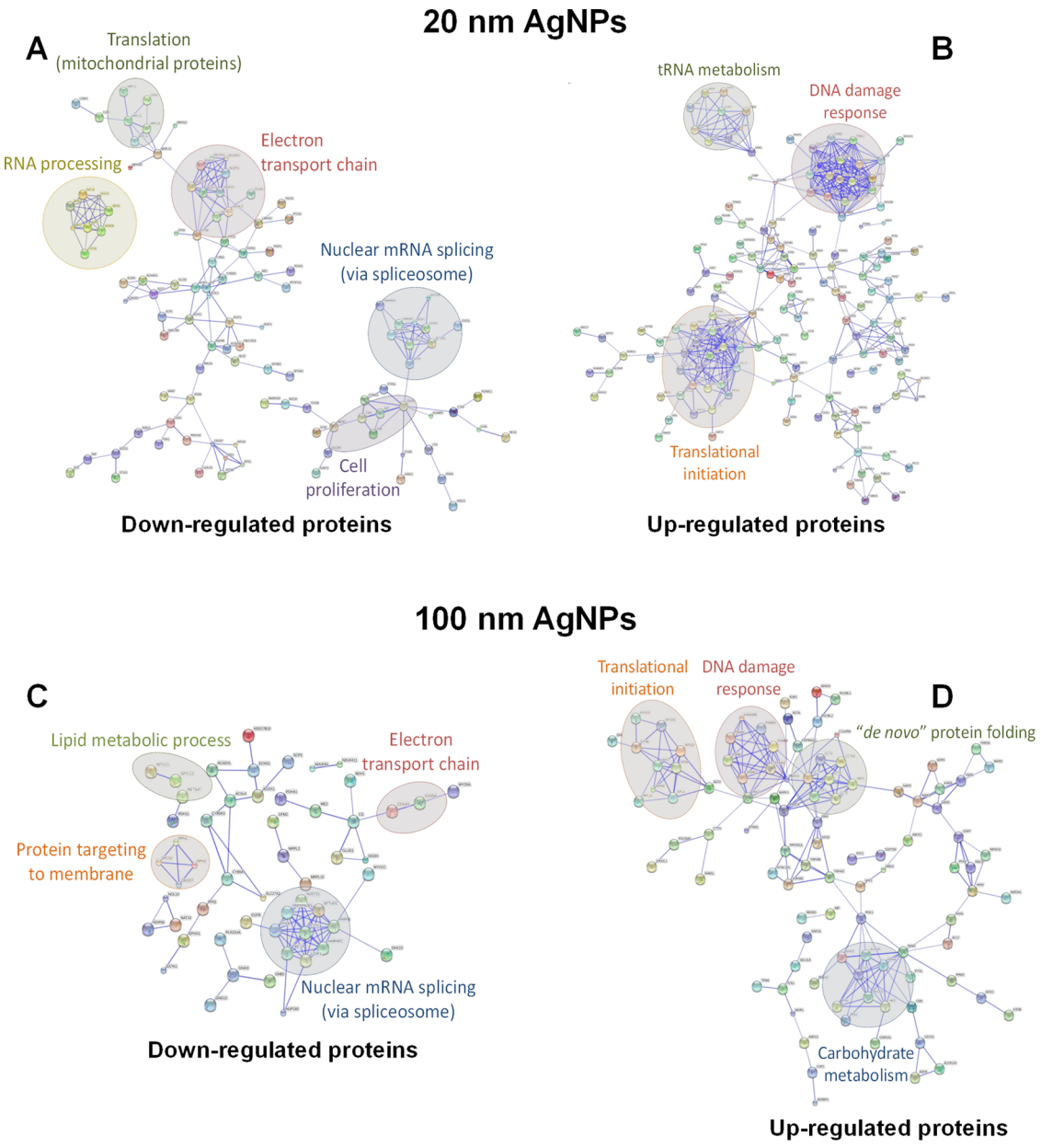

Figure 5. Protein−protein interaction networks. Functional interaction network of AgNPs regulated proteins was created by the STRING algorithm. Stronger interactions are represented by thicker lines and only high confidence interactions (score ≥ 0.7) are shown. (A) Down- and (B) up-regulated proteins induced by 24 h of 20 nm AgNPs treatment. (C) Down- and (D) up-regulated proteins induced by 24 h of 100 nm AgNPs treatment. Over-represented biological functions based on gene ontology annotation are also depicted in the figure.

in human liver cells because of exposure to 28−35 nm AgNPs.[27] Protein carbonylation due to AgNPs exposure seems to be related to the nanoparticle size since only 20 nm particles increased significantly the carbonylation levels.

The intracellular generation of ROS was also evaluated in LoVo cells after exposure with 10 μg/mL AgNPs (20 or 100 nm particle sizes) and Ag^+ ions (Ctrl 20 nm or Ctrl 100 nm) for 24 h. AgNPs (20 and 100 nm) increased the ROS levels, but the most pronounced effect was detected for the 20 nm particles, which resulted in 3 times higher ROS levels than the control (Figure 7D). The ROS levels induced by Ag^+ ions released from the nanoparticles (Ctrl 20 nm and Ctrl 100 nm) were not significantly different among them. The Ag^+ ions released from 100 nm AgNPs (Ctrl 100 nm) affected the ROS generation almost to the same extent as the nanoparticles alone (100 nm AgNPs), while the 20 nm AgNPs caused about 30% higher ROS generation than Ctrl 20 nm. Finally, 1 μg/mL Ag^+ obtained using $AgNO_3$ as the ion source revealed ROS levels in the same range as the control (Figure 7D), although 2.5 mg/mL Ag^+ caused lethal cell damage (data not shown).

ROS production and subsequent oxidative stress are reported to be an early cellular response to exposure

TABLE 2. Proteins Involved in the DNA Damage Response and Electron Transport Chain Found To Be Differentially Regulated by 20 nm AgNPs and 100 nm AgNPs

AgNPs	protein ID	gene	ratio	protein description
		Proteins Involved in the DNA Damage Response		
20 nm	P25786	PSMA1	0.42	proteasome subunit alpha type-1 isoform 2
	P25788	PSMA3	0.46	proteasome subunit alpha type-3 isoform 1
	P60900	PSMA6	0.48	proteasome subunit alpha type-6
	P20618	PSMB1	0.37	proteasome subunit beta type-1
	P28070	PSMB4	0.39	proteasome subunit beta type-4
	P28074	PSMB5	0.41	proteasome subunit beta type-5 isoform 1
	P62191	PSMC1	0.42	26S protease regulatory subunit 4
	P17980	PSMC3	0.30	26S protease regulatory subunit 6A
	P43686	PSMC4	0.42	26S protease regulatory subunit 6B isoform 1
	P62333	PSMC6	0.48	26S protease regulatory subunit 10B
	Q99460	PSMD1	0.37	26S proteasome non-ATPase regulatory subunit 1 isoform 1
	O00232	PSMD12	0.37	26S proteasome non-ATPase regulatory subunit 12 isoform 1
	O43242	PSMD3	0.49	26S proteasome non-ATPase regulatory subunit 3
	P55036	PSMD4	0.38	26S proteasome non-ATPase regulatory subunit 4
	Q16401	PSMD5	0.39	26S proteasome non-ATPase regulatory subunit 5 isoform 1
	P51665	PSMD7	0.25	26S proteasome non-ATPase regulatory subunit 7
	Q06323	PSME1	0.60	proteasome activator complex subunit 1 isoform 1
100 nm	P28066	PSMA5	0.44	proteasome subunit alpha type-5 isoform 1
	P60900	PSMA6	0.52	proteasome subunit alpha type-6
	P28070	PSMB4	0.40	proteasome subunit beta type-4
	P28072	PSMB6	0.50	proteasome subunit beta type-6 isoform 1 proprotein
	Q99436	PSMB7	0.39	proteasome subunit beta type-7 proprotein
	P62333	PSMC6	0.43	26S protease regulatory subunit 10B
	P55036	PSMD4	0.40	26S proteasome non-ATPase regulatory subunit 4
		Proteins from the Electron Transport Chain		
20 nm	P00167	CYB5A	−0.29	cytochrome b5 isoform 1
	P99999	CYCS	−0.54	cytochrome c
	Q96HE7	ERO1L	−0.38	ERO1-like protein alpha precursor
	Q86Y39	NDUFA11	−0.67	NADH dehydro. [ubiquinone] 1 α subcomplex subunit 11 isof. 1
	O43678	NDUFA2	−0.37	NADH dehydro. [ubiquinone] 1 α subcomplex subunit 2 isof. 1
	O96000	NDUFB10	−0.31	NADH dehydro. [ubiquinone] 1 β subcomplex subunit 10
	P28331	NDUFS1	−0.35	NADH-ubiqui. oxidoreduct 75 kDa subunit, mito.l isof. 1
	O75306	NDUFS2	−0.36	NADH dehydro. [ubiquinone] iron−sulfur prot 2, mito. isof. 1 precursor
	O75489	NDUFS3	−0.33	NADH dehydro. [ubiquinone] iron−sulfur prot. 3, mito. Precursor
	P49821	NDUFV1	−0.31	NADH dehydro. [ubiquinone] flavoprotein 1, mito. iso. 1 precursor
	Q9H3N1	TMX1	−0.32	thioredoxin-related transmemb. prot. 1 precursor
	Q16881	TXNRD1	0.45	thioredoxin reductase 1, cytoplasmic isoform 3
	P22695	UQCRC2	−0.31	Cytochrome *b*-c1 complex subunit 2, mitochondrial precursor
	P47985	UQCRFS1	−0.29	Cytochrome *b*-c1 complex subunit Rieske, mitochondrial
100 nm	P00167	CYB5A	−0.31	cytochrome b5 isoform 1
	Q86Y39	NDUFA11	−0.61	NADH dehydro. [ubiquinone] 1 α subcomplex subunit 11 isoform 1
	Q16718	NDUFA5	−0.35	NADH dehydro. [ubiquinone] 1 α subcomplex subunit 5

to nanoparticles and play a key role in cytotoxicity.[8,11] This is in accordance with our data since we showed that after 24 h exposure, increased levels of intracellular ROS were observed in LoVo cells treated with AgNPs and their released Ag^+ ions. This was followed by the release of cytokines, decrease of cell viability, inhibition of proliferation, and induction of apoptosis (manuscript in preparation, Miethling-Graff *et al.*).[28]

The comparison of oxidative stress caused by nanoparticles, the Ag^+ ions released from them, and the Ag^+ ions from $AgNO_3$ revealed significant differences in ROS formation. Ag^+ ions at the 1 μg/mL concentration were probably buffered by the cell medium because of its high protein content, leading to a limited increase in ROS. However, since 2.5 μg/mL Ag^+ resulted in lethal cell damage and ROS induced by Ag^+ ions released from the nanoparticles (Ctrl 20 nm and Ctrl 100 nm) led to increased ROS levels, we predict that the concentration of Ag^+ ions in Ctrl 20 nm and Ctrl 100 nm is in the range of 1−2.5 μg/mL.

Minor differences in ROS induction between 100 nm AgNPs and Ctrl 100 nm suggest that Ag^+ ions rather than the nanoparticles are responsible for the generation of ROS. However, as discussed above, the 100 nm AgNPs induced differential regulation of proteins (*e.g.*, proteins related to DNA damage and

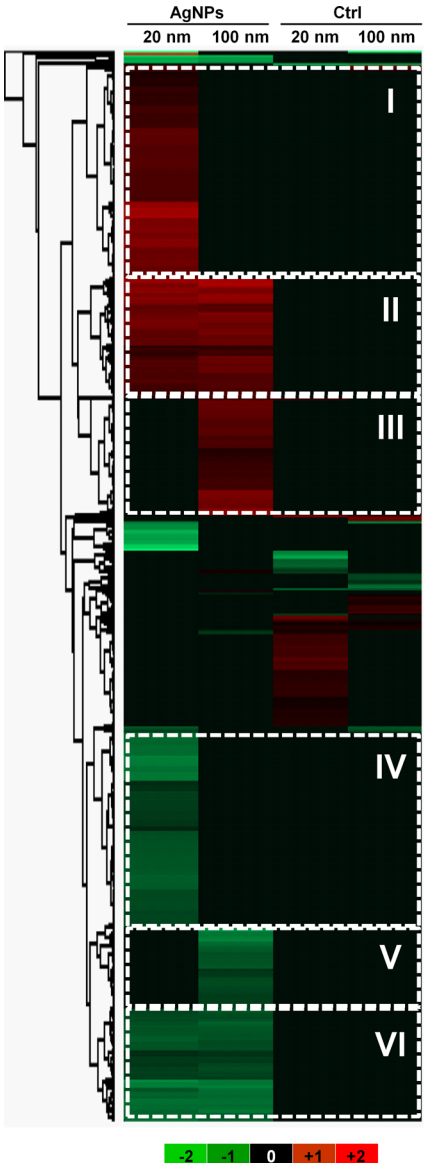

CLUSTER I			CLUSTER II		CLUSTER III		CLUSTER IV		CLUSTER V	CLUSTER VI	
AARS	PDLIM5	VCL	ADH5	TBCB	ABCE1	RUVBL2	ACADSB	MRPS22	AASS	ACOX1	SCP2
ACOT7	PNP	VCP	ALDOA	TES	ACLY	SAR1A	ACAT1	MRPS35	ACADVL	ACSL4	SLC25A5
AIMP1	PPFIBP1	WRNIP1	ANXA1	TFG	ALDH1A3	SEPT11	ACSL3	MTHFD1L	AGK	ALDH1B1	SLC3A2
AIMP2	PRDX1	YTHDF2	ANXA3	TKT	APEH	SERBP1	AGPS	MYO1B	ATL2	ATP1A1	SPTLC1
ANLN	PSMA1	YWHAG	C11orf58	TLN1	API5	SLK	ALDH2	NDUFA2	BDH1	ATP1A3	SPTLC2
ANXA11	PSMA3	YWHAQ	CCT6A	TMSB10	ARPC2	SRI	ALDH4A1	NDUFS2	C3orf26	ATP6V0A1	STRBP
AP3D1	PSMB1		CHORDC1	TPM4	ATXN2L	SRP68	ALPP	NDUFS3	CGN	CADM1	STX18
ARCN1	PSMB5		CNN3	TUBB4B	BLVRA	SUB1	AQR	NDUFV1	COX4I1	CANX	SUN2
C22orf28	PSMC1		COPB2	UPF1	CAP1	SUPT5H	ATP13A1	NOL11	CSTF3	CISD2	THOC2
CACYBP	PSMC3		DFFA	WDR77	CARM1	TCP1	ATP1B1	NSF	DNAJB11	COX5A	TIMM21
CAD	PSMC4		DSTN	XPOS	CCT4	UBA1	ATP1B3	NT5E	ECHS1	CPOX	TMF1
CEBPB	PSMD12		DYNC1H1	YARS	CCT5	UBAP2L	ATP5B	NUP155	ETHE1	CS	TOP2B
CLTB	PSMD3		EEF2	YWHAB	CCT7	VBP1	ATP5I	PDIA6	GNB2	CYB5A	VSNL1
CNBP	PSMD5		EIF4G2	YWHAE	CCT8	WARS	BAZ1B	PMPCB	GPD2	CYB5R3	WDR75
CNN2	PSMD7		ENO1	YWHAZ	CD2AP	WDR1	BCAM	PNPT1	GSTK1	DARS2	
COPA	PSME1		FDPS		CDK6		BMS1	POFUT1	HIBADH	DAZAP1	
COPG1	PTGES3		GART		CTBP1		CDC5L	PRDX4	HM13	DDOST	
DARS	RAD23B		GSR		CTTN		CIRH1A	PTK7	MIA3	DHX9	
DCAF7	RARS		GSTO1		DNM1L		CLPX	PTPMT1	MRPL2	EFTUD2	
DDX19A	RCC2		HK2		DPYSL3		CNPY2	PTPN1	MRPL37	EGFR	
DDX6	RPA1		HMGB1		EFHD2		CPSF1	PWP2	MRPL44	EPHX1	
DPYSL2	RPL12		HSP90AA1		EIF2S2		CPSF2	QSOX2	MRPS18B	ERP44	
EDC4	RPL21		HSP90AB1		EIF4B		CTNNA1	RAB10	MRPS31	GFM2	
EEF1A1	RPL24		KARS		EXOC1		CXADR	RAB11B	MYH10	GLRX5	
EEF1B2	RPL34		KIF5B		FARSA		DAD1	RAB1A	MYO1C	GLUD1	
EEF1D	RPL35A		LTA4H		FASN		DDX17	RAB35	NDUFA5	GNAI3	
EEF1G	RPL36A		MARS		FUBP1		DDX18	RAB5C	NDUFAF3	GNG12	
EIF1AX	RPS10		MCMBP		GARS		DDX21	SART1	NOMO3	HNRNPA2B1	
EIF2S1	RPS11		METTL3		GNPDA1		DDX50	SCFD1	NUP160	HNRNPC	
EIF4G1	RPS15A		MGEA5		HDLBP		DHX8	SHMT2	OGDH	HSD17B10	
EIF5B	RPS23		NAMPT		HMGB3		EMG1	SLC25A12	PCYOX1	HSD17B12	
EML4	RPS28		NANS		IMPDH1		ERO1L	SLC25A13	PLA2G4A	IARS2	
ESD	RPS3A		NMD3		IMPDH2		ESYT1	SLC9A3R1	PPIG	IMPAD1	
FARSB	RPS4X		NPLOC4		KIAA0368		EXOSC10	SLIRP	PRPF8	LAMC1	
FKBP4	RPS6		OXSR1		KIF2C		EXOSC9	SPTAN1	RAB8A	ME2	
FSCN1	SART3		PDCD6IP		LYPLA1		FASTKD2	SPTBN1	RDH11	MRPL15	
FXR1	SEPT2		PFAS		MAPK1		FAT1	STIM1	RETSAT	MRPS24	
GCN1L1	SEPT9		PFN2		MIF		FKBP8	STT3B	RPN2	MRPS28	
GFPT1	SET		PGK1		MOV10		FLOT1	TIMM9	SACM1L	NAT10	
GMPS	SH3KBP1		PPA1		MSN		FLOT2	TJP1	SCARB1	NOL10	
GTPBP1	SNX6		PRDX2		NAP1L4		GADD45GIP1	TM9SF3	SEC63	NOL9	
HDGF	SOD1		PRDX6		NARS		GOT2	TMEM70	SLC25A5	NUDT21	
HK1	SRP14		PSAT1		NASP		HADHB	TMX1	SLC27A2	NVL	
HSPA4	SRP9P1		PSMA6		OLA1		HEATR1	TRAP1	SMC1A	OSBPL8	
HSPH1	SRRM2		PSMB4		OSBP		HEXA	TRMT10C	SMPD4	PDHA1	
IPO7	SSB		PSMC6		PAICS		HIBCH	UQCRC2	SPCS2	PGAM5	
IQGAP1	ST13		PSMD4		PAK2		HIP1	UQCRFS1	TAF15	PGRMC1	
LARS	STIP1		PYGL		PCBP2		HNRNPA3	URB2	TARDBP	PIGS	
LIMS1	SUMO2		RBM12		PFKL		HNRNPAB	UTP18	TECR	PLOD3	
LRRC47	TCOF1		RNH1		PFKM		HSD17B11	UTP20	TMED10	PLXNB2	
MAD2L1	TPM3		RPAP3		PFN1		HSD17B4	VDAC3	TMED9	PMPCA	
MAP4	TPX2		RTF1		PKM		HSPD1	VRK1	TRAM1	PODXL	
MTAP	TRIM25		RUVBL1		PPAT		ITGA6	WBSCR16	TRRAP	POLDIP2	
MTHFD1	TRIM28		SARS		PPM1G		JUP	WDR3	TSPAN8	PRDX3	
MYH9	TSNAX		SEC31A		PPP2CA		LGALS3	WDR36	U2AF1	PRPF4B	
NUDC	TSR1		SFN		PPP2R1A		LONP1	XRN2	UTRN	PTCD3	
NUSAP1	TUBA1C		SGTA		PSMA5		LRPPRC	YME1L1	ZNF638	RAB14	
PA2G4	TUBA4A		SH3GL1		PSMB6		LYN			RAB18	
PABPC1	TUBB		STMN1		PSMB7		MCAT			RAB23	
PABPC4	TUBB2A		STRAP		RAN		MCCC2			RAB7L1	
PCMT1	TXNRD1		SYAP1		RPS20		MRPL11			RHOG	
PDAP1	UBR4		TAGLN2		RPS7		MRPL24			RPN1	
PDLIM1	VARS		TALDO1		RRM2		MRPL45			SAMM50	

Figure 6. Hierarchical clustering of proteins differentially regulated by AgNPs and Ag^+-containing supernatants. Cluster I, proteins up-regulated by 20 nm AgNPs treatment. Cluster II, proteins up-regulated by both particle sizes. Cluster III, proteins up-regulated by 100 nm AgNPs treatment. Cluster IV and V, proteins down-regulated after 20 or 100 nm AgNPs treatment, respectively. Cluster VI, proteins up-regulated by both particle sizes.

apoptosis) that were not regulated by exposure to Ctrl 100 nm, indicating that the nanoparticle itself indeed induced cellular stress. In sharp contrast, there is no doubt that ROS generation and the cytotoxicity induced by 20 nm particles were primarily caused by the nanoparticle effects, although an Ag^+ contribution cannot be ignored. This is in accordance with a previous study reporting that the oxidative stress induced by ROS was most pronounced with AgNPs (particle sizes of 30 and 50 nm) than with of Ag^+ ions.[29]

The OxyBlot and ROS data suggest that the ROS produced due to 100 nm particles was completely scavenged by the intracellular oxidation−reduction system, whereas the higher ROS levels induced by 20 nm AgNPs disrupted cellular homeostasis, leading to increases in protein carbonylation.

Size-Dependent Cellular uptake of AgNPs. We used confocal laser scanning microscopy (CLSM) to record three-dimensional pictures of LoVo cells exposed to AgNPs. This technology offers sufficient resolution to visualize extracellular or intracellular nanoparticles. The CLSM data revealed that the 20 nm particles were assimilated by the cells and large clusters of aggregated nanoparticles could be observed (Figure 8a). Moreover, the 20 nm nanoparticles also induced morphological changes in the LoVo cells, which included rounded shapes indicating cellular stress. Only a few 100 nm particles entered the LoVo cells after 24 h exposure. Instead, most of the 100 nm nanoparticles were located on the plasma membrane (Figure 8b). Diverging data regarding nanoparticle size and cellular uptake rate is available in the literature. Although

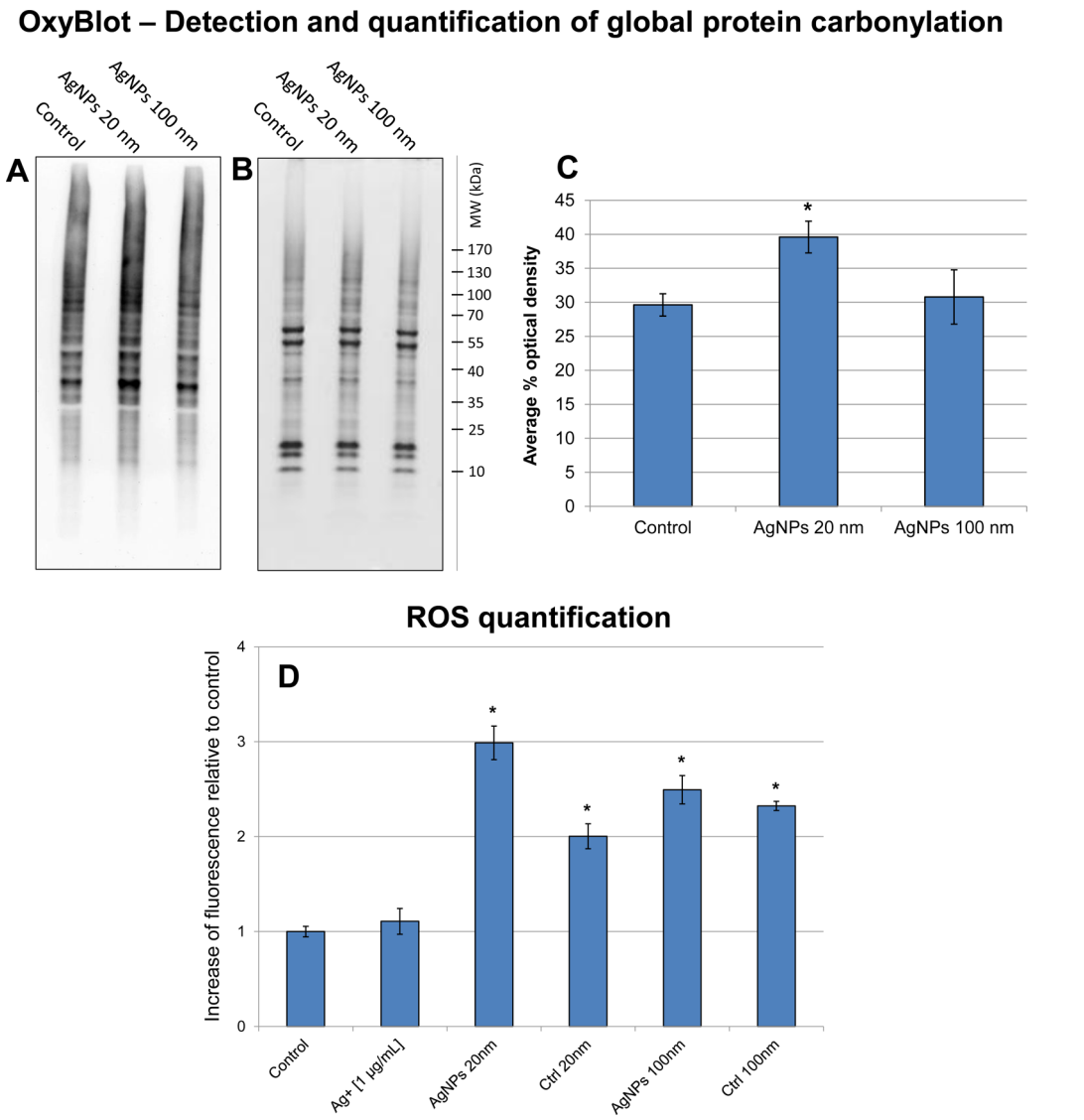

Figure 7. Cellular oxidative stress induced by AgNPs. (A) OxyBlot detection of carbonylated proteins. (B) Loading control visualized with Coomassie Brilliant Blue total protein stain. (C) Levels of protein carbonylation expressed as average % optical density. (D) Effects of AgNPs on the intracellular ROS levels. ROS was evaluated after 24 h of exposure by H_2DCF-DA staining using flow cytometry. Data represent the increase in fluorescence relative to controls and are expressed as means ± SD. Asterisk (*) denotes significant differences compared to the controls ($p < 0.05$); $n = 2$ for OxyBlot analysis and $n = 5$ for ROS assay.

there are a number of studies reporting that smaller nanoparticles have higher uptake rates than larger ones,[7,10,30,31] which is in line with our observations, there are studies reporting that nanoparticles larger than 100 nm readily enter inside the cells.[26,32] It is therefore clear that the cellular uptake is a complex mechanism driven not only by the nanoparticles size but also by *e.g.*, their shapes, coating materials and protein coronas.[11,33]

Recently, it was proposed that AgNPs can be internalized by macrophages *via* scavenger receptors.[9,34] Although it is still necessary to address whether scavenger receptors are involved in LoVo cell uptake of AgNPs, the scavenger receptor class B member 1 (GFM2) was differentially down-regulated only after 100 nm AgNPs exposure (Supporting Information Table 2), suggesting that this receptor may play a role in the uptake of 20 nm particles.

Once inside the cells, the smaller nanoparticles can interact with proteins (forming protein coronas[11,33]), disrupt cellular metabolism and homeostasis, and induce damage while the 100 nm particles may have more indirect effects on cells. The same argument is valid for the higher production of ROS observed for 20 nm particles and the subsequent higher levels of oxidative stress. Different mechanisms of action for nanoparticles either as particles or because of the Ag^+ ions that they release have been proposed. For example, Park *et al.* suggested a Trojan-horse-type mechanism for silver nanoparticles in the macrophage cell line RAW264.7 that causes ionization of AgNPs after phagocytosis,[35] a mechanism that was also proposed

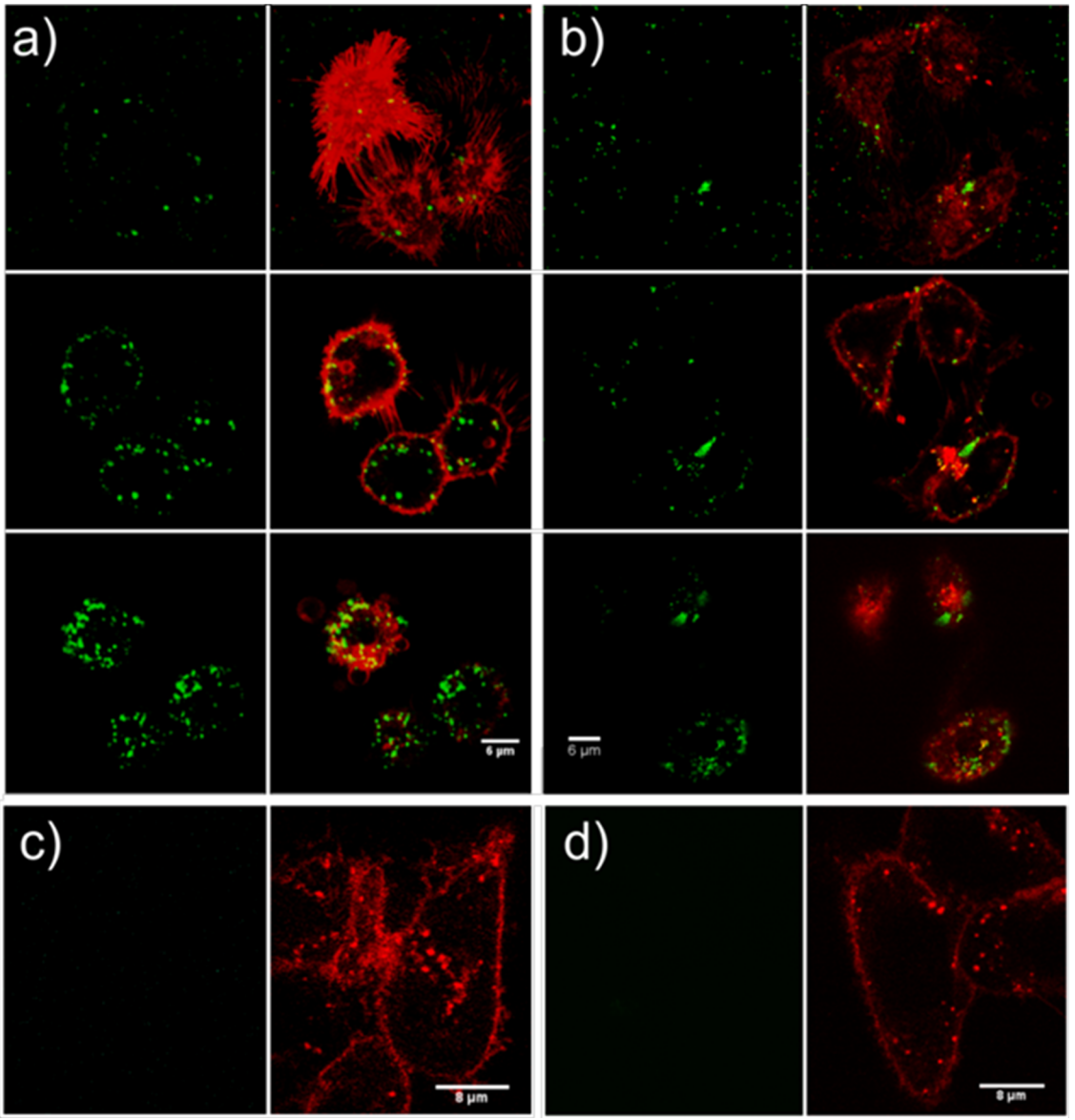

Figure 8. Confocal laser scanning microscopy of LoVo cells stimulated with 20 and 100 nm AgNPs. (a and b) Green dots represent AgNPs and red dots represent the plasma membrane stained with the fluorescent membrane marker DiI c18. Yellow, reflects overlap regions of AgNPs (green) with plasma membrane (red). Images on the top row represent the bottom of the cell, the middle row images are 4 μm into the cell, and the bottom row shows the top of the cell. Panel a depicts the uptake of 20 nm AgNPs, imaged by two photon excited emission (see Methods and Supporting Information Figure S4). Panel b shows the uptake of 100 nm AgNPs imaged by reflection of the excitation laser. The images show that the 20 nm particles are mobilized into the cell, where they are concentrated in clusters. The 100 nm particles are primarily found on the cell surface. The images shown are representative of more than 30 cells. Panel c shows an image of cells without nanoparticles taken under the same conditions as the images for the 20 nm AgNPs. Panel d shows an image of cells without nanoparticles taken under the same conditions as the images for the 100 nm AgNPs. Panels c and d implicate that the signal in panels a and b is not inherent to the cells but comes from the AgNPs.

by Singh and Ramarao.[9] Conversely, Kim *et al.* indicated that AgNPs-induced toxicity is an intrinsic effect independent of free Ag^+ ions with different mechanisms for AgNPs and ions, because the oxidative stress-related mRNA species were regulated in different ways.[36] Our results point in the same direction, suggesting that the cellular response to AgNPs exposure is the sum of events triggered by a direct effect of the nanoparticles and an indirect effect of free Ag^+ ions released from the nanoparticles. Furthermore, our data suggests different modes of action depending upon the AgNPs particle size. The 20 nm particles are entering LoVo cells and induce a direct effect on cellular proteins and metabolism, leading to up-regulation of protein SUMOylation and ubiquitination pathways and down-regulation of important proteins from the electron transport chain. By contrast, the 100 nm particles induce an indirect effect on cells, probably by way of a yet to be identified receptor that triggers kinase (*i.e.*, MAPK and PAK) and phosphatase (phosphatase 2A)

pathways, leading to up-regulation of proteins from the ubiquitination−proteasome system and down-regulation of proteins from the electron transport chain. The effects of both particle sizes on cells are similar, although more prominent for the 20 nm particles, and include ROS generation, DNA damage, protein carbonylation, and apoptosis.

CONCLUSIONS

Mass spectrometry-based proteomics study of human cells exposed with silver nanoparticles demonstrated that the size of the nanoparticle is a crucial feature that determines the type and magnitude of the cellular response. In general, the smaller particles induce a greater response to the protein network. Part of the explanation for this size dependence can be attributed to the 20 nm particles that are entering human cells, whereas 100 nm nanoparticles mainly remain outside the cell interacting with the plasma membrane. This is consistent with a higher concentration of intracellular ROS in cells treated with 20 nm AgNPs than that in cells treated with 100 nm AgNPs. We also demonstrated that proteins can be differentially regulated by both nanoparticles and the free silver ions can be released by nanoparticles. However, the nanoparticles and the ions influence different sets of proteins and many more proteins were regulated by nanoparticles than by the Ag^+ ions, which reveal that nanoparticles play a key role in inducing cellular stress. Results also show that protein ubiquitination and degradation *via* the proteasome complex is triggered by both 20 and 100 nm nanoparticles. Finally, we provide evidence for increased protein SUMOylation after exposure of cells to 20 nm AgNPs and activation of the MAPK1, PAK2 and phosphatase 2A signaling cascades after exposure to 100 nm AgNPs. These are significant responses to AgNPs in human cells and results provide new insights to the mechanism of nanoproteome interactions.

METHODS

Reagents. Trypsin was from Promega (Fitchburg, MI). The iTRAQ 8-plex reagents were from Applied Biosystems (Foster City, CA). Ammonia solution (25%) was from Merck (Darmstadt, Germany). Tris was from Plus One, GE Healthcare (Brondby, Denmark). Amicon ultra-0.5 mL centrifuge filters (10 kDa) were from Merck Millipore (Darmstadt, Germany). Ammonium formate, sodium dodecyl sulfate (SDS), DL-dithiothreitol (DTT), urea, iodoacetamide (IAA), and triethylammonium bicarbonate buffer (TEAB) were obtained from Sigma (Steinheim, Germany).

Silver Nanoparticles (AgNPs). Spherical silver nanoparticles (NanoXactTM), 20 and 100 nm, using citrate as capping-agent, were purchased from Nanocomposix (San Diego, CA). The mass concentration was 0.02 mg/mL in 2 mM citrate buffer. The particle diameters (TEM) exhibited a narrow size distribution with less than 12% deviation for each lot. SEM-EDX analysis revealed no impurities in the elemental composition of the nanoparticles. The stability of the nanoparticles in solution (2 mM citrate buffer) was measured with dynamic laser scattering (DLS) over time using different batches (DAC1212, DAC1406, DAC1110 and JMW1476) and no significant changes (*i.e.*, size and ζ-potential) were observed (CV < 4%). Before the addition of AgNPs in the cell medium for the exposure experiments, the stock solutions containing AgNPs were filtered through a 0.22 μm PVDS syringe filter (Roth, Karlsruhe, Germany) to avoid bacterial contamination.

Dynamic Laser Scattering (DLS) Analyses. Nanoparticles size and ζ-potential were determined from the nanoparticle stock solutions (0.02 mg/mL in 2 mM citrate buffer) using the instrument DelsaMax Pro (Beckman Coulter, Brea, CA).

LoVo Cell Culture and AgNPs Exposure Protocol. The human colon carcinoma cell line LoVo (ACC 350, German Collection of Microorganisms and Cell Cultures-DSMZ, Germany) was grown as monolayer in RPMI 1640 medium with stable glutamine supplemented with 10% fetal bovine serum (FBS) Superior (Biochrom, Berlin, Germany) at 37 °C in a 5% CO_2 humidified atmosphere. Passages 9−13 were used for cytotoxicological analyses.

A total of 3 and 5 × 10^5/mL cells were pregrown for 24 h in T75 flasks for proteome and OxyBlot analyses and 12-well plates for ROS measurement, respectively. After removal of the culture medium, exposure of AgNPs was initiated by adding fresh culture medium containing AgNPs. The dose of AgNPs and Ag^+ ions using $AgNO_3$ as ion source was calculated based on silver mass and adjusted by dilution of the AgNPs stock solution with cell culture medium at the start of exposure.

To investigate the toxic effect of Ag^+ ions released from AgNPs within 24 h, RPMI 1640 medium with FBS (10%) containing AgNPs at a concentration of 10 μg/mL was incubated under cell growth conditions for 24 h before the actual experiment. Thereafter, AgNPs were separated from 15 mL of medium from each T75 flask by centrifugation (20 nm AgNPs, 2 × 7.5 mL medium for 150 min at 4300*g*; AgNPs 100 nm, 2 × 7.5 mL medium for 10 min at 4300*g* Heraeus Contifuge Stratos, ThemoFisher Scientific, Germany). The supernatant containing silver ions released from 20 nm AgNPs (Ctrl 20 nm) and 100 nm AgNPs (Ctrl 100 nm), respectively, was added to the pregrown cells to begin exposure.

For proteome analysis, the medium was removed at the end of exposure and cells were washed three times with PBS. Next, 10 mL of ice-cold PBS was added and cells were harvested using a cell scraper. Cell suspensions were transferred to 15 mL Falcon tubes, centrifuged for 3 min at 500*g* and frozen at −80 °C until further analysis.

Cell Lysis and In-Filter Protein Digestion. LoVo cells were lysed and proteins digested essentially as previously described[37,38] with minor modifications. Briefly, LoVo cells were incubated at room temperature with 4% SDS/0.1 M Tris-HCl (pH 7.6)/0.1 M DTT. Cell lysis was enhanced and DNA filaments were sheared by tip sonication on ice. Following the exchange of SDS-containing by urea-containing solution (8 M urea/0.1 M Tris-HCl, pH 8.5), and alkylation of the reduced thiol groups with 0.05 M IAA in the dark for 30 min, the solution was exchanged with 50 mM TEAB and proteins were digested in-filter with trypsin (50:1) for 18 h at room temperature. Peptides were collected in new collection tubes and the filter units were washed with 0.5 M ammonium formate. The samples were lyophilized to evaporate the ammonium formate.

Peptide Labeling. Peptides (30 μg) were labeled with iTRAQ 8-plex reagent according to manufacturer's specifications. We used different iTRAQ tags to label peptides from the same experimental condition over the three biological replicates to avoid any bias specific to an isobaric reagent. The tags used to label the peptides from each experimental condition were as follows: control (113, 115 and 118), 20 nm AgNPs (114, 116 and 119), 100 nm AgNPs (115, 117 and 121), Ctrl 20 nm (113, 116 and 118), and Ctrl 100 nm (114, 117 and 119). Peptides were combined 1:1:1:1:1 and lyophilized.

HILIC Fractionation. Before LC−MS/MS analysis, samples were prefractionated on a TSKGel Amide 80 HILIC HPLC column (length, 15 cm; diameter, 2 mm; particle size, 3 μm) to reduce complexity and to remove unbound iTRAQ reagents. Samples (approximately 30 μg) were resuspended in solvent B (90% acetonitrile (ACN), 0.1% trifluoroacetic acid (TFA)) and peptides were eluted at 6 μL/min by decreasing solvent B in a linear manner (100−60%) over 26 min. Ten fractions were collected and lyophilized.

Reversed-Phase NanoLC-ESI MS/MS. Nanoliquid chromatography coupled to tandem MS (nano-LC−MS/MS) analysis was performed using an Easy-LC nanoHPLC (Thermo Fisher, Waltham, MA) interfaced with a Thermo LTQ Orbitrap Velos MS (Thermo Fisher, Waltham, MA). HILIC fractions were resuspended with 0.1% formic acid (FA) and a volume corresponded to 600 mAU of each HILIC fraction was loaded onto a 5 cm × 100 μm (length × inner diameter) precolumn packed in-house with 5 μm (particle size) Reprosil-Pur C18-AQ resin (Dr. Maisch GmbH, Ammerbuch, Germany). The 17 cm × 75 μm (length × inner diameter) analytical column was packed in-house with 3 μm (particle size) Reprosil-Pur C18-AQ resin (Dr. Maisch GmbH, Ammerbuch, Germany). To avoid the supercharged effect of the iTRAQ 8-plex,[17] a 5% ammonia solution was placed under the electrospray needle. The chromatography gradient was 0−34% solvent B (90% ACN, 0.1% FA) over 163 min at a flow rate of 300 nL/min. The mass spectrometer was operated in data-dependent mode. The seven most intense precursor ions from each MS1 survey scan (300−1800 *m/z*; 30 000 resolution at 400 *m/z*) were selected (isolation width = 2 Th) to be fragmented with HCD (normalized collision energy = 48%, activation time = 0.1 ms). The MS2 fragment ions were resolved in the Orbitrap mass analyzer (7500 resolution at 400 *m/z*). For the full scan (MS1), ions were accumulated in the Orbitrap until reaching either a target value of 10^6 ions or a maximum filling time of 500 ms. For MS2 scans, the automatic gain control (AGC) was set to allow either 10^5 ions or a 300 ms injection time. Detected ions (±10 ppm mass window) were included in the dynamic exclusion list for 40 s (max 500 ions) and singly charged precursor ions were not selected for fragmentation. Raw data were viewed in Xcalibur v2.0.7 (Thermo Fisher; Waltham, MA).

Data Processing and Database Searching. The MS/MS spectra were processed (smoothing, background subtraction, and centroiding) using Proteome Discoverer version 1.3 beta (Thermo Fisher, Waltham, MA) and database searches were performed against a target and decoy (reverse) separated *Homo sapiens* database downloaded from Swiss-Prot (Sprot 2012_07 version; 536 789 sequences; 190 518 892 residues) using an in-house Mascot server (version 2.3.0; Matrix Science Ltd., London, U.K.). Trypsin was chosen as the enzyme allowing up to two missed cleavage sites. The precursor mass tolerance was set to ±10 ppm, although for HCD MS/MS spectra the fragment mass tolerance was set to ±0.08 Da. Methionine oxidation and iTRAQ 8-plex (K and N-terminal) were chosen as dynamic modifications and carbamidomethyl cysteine was chosen as static modification. The global peptide false discovery rate (FDR) was calculated by using the Percolator algorithm.[39] Only rank 1 peptides and with global FDR ≤ 1% were used in this study.

Data Normalization and Significance Analysis. The peptides identified in the three independent biological replicates had their intensities $\log_2$-transformed and normalized based on the median. The R Rollup function from the DanteR package (http://www.omics.pnl.com) was used to merge peptides from the same protein using the mean. The common quantitative approach consists in comparison of the ratios of the three replicates. In an equivalent way, we subtracted the mean over the five experimental conditions for each protein in each replicate, decreasing the influence of measurement errors of the first condition. Significant up/down-regulations between experimental conditions were determined by *p*-values. The values were calculated using the one-way analysis of variance (ANOVA) procedure of the DanteR software and corrected for multiple testing with Benjamini−Hochberg.[40] Only proteins with *p*-value ≤0.01 were considered differentially regulated.

Proteomic Data Availability. Raw LC−MS/MS output files, annotated MS/MS spectra and Excel table sheets containing all peptides identified in the three biological replicates are available for download at: http://nanoproteomics.s3.amazonaws.com/list.html. We recommend first reading the README file, which contains important information about the data deposited.

ROS Measurements. The intracellular generation of ROS was evaluated using the fluorescence marker H_2DCF-DA (2′,7′-dichlorodihydrofluoresein diacetate) as previously described[8] with minor modifications. Briefly, a total of 5 × 10^5 cells were seeded in 12-well plates and preincubated for 24h. After 24 h exposure to AgNPs, cells were washed once with PBS and subsequently stained with 1 mL of 5 μM H_2DCF-DA for 30 min in the dark at 37 °C/5% CO_2. After removal of the staining solution and washing with PBS, cells were trypsinized, centrifuged, resuspended, and analyzed using a FACScan flow cytometer (Becton Dickinson, Mountain View, CA). For excitation, an argon laser with a wavelength of 488 nm was used and fluorescent DCF was analyzed at an emission wavelength of 530/30 nm. Flow cytometry configuration, standard compensation, and data acquisition used CellQuestTMPro software suite provided by Becton Dickinson. A total of 5,000 events were collected for each analysis. Raw data were further analyzed using CyflogicTM software.

Data are expressed as mean ± SD of at least five independent experiments. Statistical analyses were performed using SigmaPlot V. 11.0. Differences among AgNPs treated samples and untreated controls were tested by one-way ANOVA followed by Holm-Sidak test. The *p*-values ≤0.05 were considered to be statistically significant.

Western Blot and OxyBlot. Cells were lysed in 20 mM TEAB, 4% SDS, 1 mM EDTA buffer using tip sonication. Samples were separated in a Bolt4−12% Bis-Tris Plus gel using Bolt MES SDS Running Buffer (Invitrogen, Carlsbad, CA) following manufacturer's instructions. Separated proteins were electro-transferred onto an Immobilon-P Membrane, PVDF (Merck Millipore, Darmstadt, Germany). Primary antibody binding was detected by incubation with a peroxidase-conjugated secondary antibody and chemiluminescent substrate Luminata Forte (Merck Millipore, Darmstadt, Germany). Carbonylated proteins were detected and analyzed after derivatization of protein carbonyl groups with 2,4-dinitrophenylhydrazine using the OxyBlot kit - (Merck Millipore, Darmstadt, Germany). Immunodetection was performed with 7.5 μg of protein per lane and a primary antibody directed against dinitrophenylhydrazone. Loading control used the same amount of samples separated by SDS−PAGE under the same conditions and stained with sensitive Coomassie Blue stain.[41]

Density analysis was performed using Image Studio Light (Li-Cor). The optical density for each lane was normalized to the total density of all lanes on the gel and expressed as % optical density. Data are expressed as mean ± SD of two independent experiments. Statistical analysis was performed by Student's *t*-test and only changes with *p*-values ≤0.05 were considered significant.

Samples for Imaging. A total of 5 ×10^5 LoVo cells were pregrown in CELLview dishes (Greiner Bio-One, Germany) for 24 h. After subsequent exposure to AgNPs, 20 or 100 nm at 10 μg/mL, medium was removed and cells were stained by using DiI (1,1′-dioctadecyl-3,3,3′,3′-tetramethylindocarbocyanine perchlorate ('DiI'; DiIC18(3)) as lipophilic membrane dye (Life technologies, Molecular Probes, Carlsbad, CA). Five microliters of DiI (1 mM in ethanol) diluted in 1 mL of cell culture medium without phenol red was used for staining the cells for 20 min at 37 °C. Cells were washed three times with fresh medium allowing for 10 min recovery before proceeding. Finally, 1 mL of medium without phenol red was added and cells were stored at 2−8 °C until they were analyzed by microscopy.

Confocal Microscopy. Confocal imaging was carried out on a Zeiss LSM 510 META. The samples were imaged using a 63 × 1.4 NA oil immersion objective (Carl Zeiss). For the 100 nm nanoparticles, the excitation laser was a 543 nm HeNe laser, and they were imaged by detecting their reflection of the

excitation laser. The reflection of the laser from the AgNPs was collected through a 500−550 nm band-pass filter. The 20 nm nanoparticles were imaged using a femtosecond pulsed laser (Mai Tai broad band, Spectra Physics, Mountain View, CA) operated at 800 nm. The multiphoton excited emission of AgNPs has been previously demonstrated[42,43] (see also Supporting Information and Figure S4). The emission was collected through a 685 nm short pass filter. Control measurements were performed to ensure that only the AgNPs were imaged in the channel designated for recording the nanoparticles. The fluorescent emission from the DiI was collected through a 560 nm long pass filter. The images shown are representative of more than 30 cells.

Conflict of Interest: The authors declare no competing financial interest.

Acknowledgment. This work was supported by INTERREG 4A Syddanmark-Schleswig-K.E.R.N. and the Danish Council for Independent Research, Natural Sciences (FNU grant FK272-08-0044). The authors are thankful to V. Schwämmle for sharing his knowledge of statistical analysis. For the DLS measurements, we would like to thank P. Hervella and the Danish National Research Foundation Niels Bohr Visiting Professorship to SDU for providing the Beckmann Coulter Delsa Max Pro in the Center for Single Particle Science and Engineering (SPSE).

Supporting Information Available: Proteomics reproducibility; proteomics statistical analysis output; protein−protein interacting networks; images of emission from 20 nm AgNPs excited by 800 nm femtosecond pulsed light and emission spectrum;.list of all proteins identified in the study; list of differentially regulated proteins. This material is available free of charge *via* the Internet at http://pubs.acs.org.

REFERENCES AND NOTES

1. Lara, H. H.; Garza-Trevino, E. N.; Ixtepan-Turrent, L.; Singh, D. K. Silver Nanoparticles Are Broad-Spectrum Bactericidal and Virucidal Compounds. *J. Nanobiotechnol.* **2011**, *9*, 30.
2. You, C.; Han, C.; Wang, X.; Zheng, Y.; Li, Q.; Hu, X.; Sun, H. The Progress of Silver Nanoparticles in the Antibacterial Mechanism, Clinical Application and Cytotoxicity. *Mol. Biol. Rep.* **2012**, *39*, 9193–9201.
3. PEN Consumer Products. An Inventory of Nanotechnology Based Consumer Products Currently on the Market. Available online at http://www.nanotechproject.org.
4. Kim, Y. S.; Kim, J. S.; Cho, H. S.; Rha, D. S.; Kim, J. M.; Park, J. D.; Choi, B. S.; Lim, R.; Chang, H. K.; Chung, Y. H.; *et al.* Twenty-Eight-Day Oral Toxicity, Genotoxicity, and Gender-Related Tissue Distribution of Silver Nanoparticles in Sprague-Dawley Rats. *Inhalation Toxicol.* **2008**, *20*, 575–583.
5. Kim, W. Y.; Kim, J.; Park, J. D.; Ryu, H. Y.; Yu, I. J. Histological Study of Gender Differences in Accumulation of Silver Nanoparticles in Kidneys of Fischer 344 Rats. *J. Toxicol. Environ. Health, Part A* **2009**, *72*, 1279–1284.
6. Carlson, C.; Hussain, S. M.; Schrand, A. M.; Braydich-Stolle, L. K.; Hess, K. L.; Jones, R. L.; Schlager, J. J. Unique Cellular Interaction of Silver Nanoparticles: Size-Dependent Generation of Reactive Oxygen Species. *J. Phys. Chem. B* **2008**, *112*, 13608–13619.
7. Kim, T. H.; Kim, M.; Park, H. S.; Shin, U. S.; Gong, M. S.; Kim, H. W. Size-Dependent Cellular Toxicity of Silver Nano particles. *J. Biomed. Mater. Res., Part A* **2012**, *100*, 1033–1043.
8. AshaRani, P. V.; Low Kah Mun, G.; Hande, M. P.; Valiyaveettil, S. Cytotoxicity and Genotoxicity of Silver Nanoparticles in Human Cells. *ACS Nano* **2009**, *3*, 279–290.
9. Singh, R. P.; Ramarao, P. Cellular Uptake, Intracellular Trafficking and Cytotoxicity of Silver Nanoparticles. *Toxicol. Lett.* **2012**, *213*, 249–259.
10. Bouwmeester, H.; Poortman, J.; Peters, R. J.; Wijma, E.; Kramer, E.; Makama, S.; Puspitaninganindita, K.; Marvin, H. J.; Peijnenburg, A. A.; Hendriksen, P. J. Characterization of Translocation of Silver Nanoparticles and Effects on Whole-Genome Gene Expression Using an *in Vitro* Intestinal Epithelium Coculture Model. *ACS Nano* **2011**, *5*, 4091–4103.
11. Lai, Z. W.; Yan, Y.; Caruso, F.; Nice, E. C. Emerging Techniques in Proteomics for Probing Nano−Bio Interactions. *ACS Nano* **2012**, *6*, 10438–10448.
12. Greulich, C.; Kittler, S.; Epple, M.; Muhr, G.; Koller, M. Studies on the Biocompatibility and the Interaction of Silver Nanoparticles with Human Mesenchymal Stem Cells (HMSCs). *Langenbecks Arch. Surg.* **2009**, *394*, 495–502.
13. Kittler, S. C. G.; Gebauer, J. S.; Diendorf, J.; Treuel, L.; Ruiz, L.; Gonzalez-Calbet, J. M.; Vallet-Regi, M.; Zellner, R.; Köller, M.; Epple, M. The Influence of Proteins on the Dispersability and Cell-Biological Activity of Silver Nanoparticles. *J. Mater. Chem.* **2009**, *20*, 512–518.
14. Ross, P. L.; Huang, Y. N.; Marchese, J. N.; Williamson, B.; Parker, K.; Hattan, S.; Khainovski, N.; Pillai, S.; Dey, S.; Daniels, S.; *et al.* Multiplexed Protein Quantitation in Saccharomyces Cerevisiae Using Amine-Reactive Isobaric Tagging Reagents. *Mol. Cell. Proteomics* **2004**, *3*, 1154–1169.
15. Kittler, S.; Greulich, C.; Diendorf, J.; Köller, M.; Epple, M. Toxicity of Silver Nanoparticles Increases During Storage Because of Slow Dissolution under Release of Silver Ions. *Chem. Mater.* **2010**, *22*, 4548–4554.
16. Gilar, M.; Olivova, P.; Daly, A. E.; Gebler, J. C. Orthogonality of Separation in Two-Dimensional Liquid Chromatography. *Anal. Chem.* **2005**, *77*, 6426–6434.
17. Thingholm, T. E.; Palmisano, G.; Kjeldsen, F.; Larsen, M. R. Undesirable Charge-Enhancement of Isobaric Tagged Phosphopeptides Leads to Reduced Identification Efficiency. *J. Proteome Res.* **2010**, *9*, 4045–4052.
18. Szklarczyk, D.; Franceschini, A.; Kuhn, M.; Simonovic, M.; Roth, A.; Minguez, P.; Doerks, T.; Stark, M.; Muller, J.; Bork, P.; *et al.* The String Database in 2011: Functional Interaction Networks of Proteins, Globally Integrated and Scored. *Nucleic Acids Res.* **2011**, *39*, D561–568.
19. Nishikawa, H.; Ooka, S.; Sato, K.; Arima, K.; Okamoto, J.; Klevit, R. E.; Fukuda, M.; Ohta, T. Mass Spectrometric and Mutational Analyses Reveal Lys-6-Linked Polyubiquitin Chains Catalyzed by Brca1-Bard1 Ubiquitin Ligase. *J. Biol. Chem.* **2004**, *279*, 3916–3924.
20. Chu, Y.; Yang, X. Sumo E3 Ligase Activity of Trim Proteins. *Oncogene* **2011**, *30*, 1108–1116.
21. Muller, S.; Hoege, C.; Pyrowolakis, G.; Jentsch, S. Sumo, Ubiquitin's Mysterious Cousin. *Nat. Rev. Mol. Cell Biol.* **2001**, *2*, 202–210.
22. Rudel, T.; Bokoch, G. M. Membrane and Morphological Changes in Apoptotic Cells Regulated by Caspase-Mediated Activation of Pak2. *Science* **1997**, *276*, 1571–1574.
23. Gabai, V. L.; Yaglom, J. A.; Volloch, V.; Meriin, A. B.; Force, T.; Koutroumanis, M.; Massie, B.; Mosser, D. D.; Sherman, M. Y. Hsp72-Mediated Suppression of C-Jun N-Terminal Kinase Is Implicated in Development of Tolerance to Caspase-Independent Cell Death. *Mol. Cell. Biol.* **2000**, *20*, 6826–6836.
24. Eom, H. J.; Choi, J. P38 Mapk Activation, DNA Damage, Cell Cycle Arrest and Apoptosis as Mechanisms of Toxicity of Silver Nanoparticles in Jurkat T Cells. *Environ. Sci. Technol.* **2010**, *44*, 8337–8342.
25. Janssens, V.; Rebollo, A. The Role and Therapeutic Potential of Ser/Thr Phosphatase Pp2a in Apoptotic Signalling Networks in Human Cancer Cells. *Curr. Mol. Med.* **2012**, *12*, 268–287.
26. Yan, Y.; Lai, Z. W.; Goode, R. J.; Cui, J.; Bacic, T.; Kamphuis, M. M.; Nice, E. C.; Caruso, F. Particles on the Move: Intracellular Trafficking and Asymmetric Mitotic Partitioning of Nanoporous Polymer Particles. *ACS Nano* **2013**, *7*, 5558–5567.
27. Piao, M. J.; Kang, K. A.; Lee, I. K.; Kim, H. S.; Kim, S.; Choi, J. Y.; Choi, J.; Hyun, J. W. Silver Nanoparticles Induce Oxidative Cell Damage in Human Liver Cells through Inhibition of Reduced Glutathione and Induction of Mitochondria-Involved Apoptosis. *Toxicol. Lett.* **2011**, *201*, 92–100.
28. Miethling-Graff, R.; Rumpker, R.; Richter, M.; Verano-Braga, T.; Kjeldsen, F.; Brewer, J.; Rubahn, H. G.; Erdmann, H.

Exposure to Silver Nanoparticles Induces Size-and Dose-Related Oxidative Stress and Cytotoxicity in Human Colon Carcinoma Cells. *Toxicol. In Vitro*, submitted for pubication, **2014**.
29. Foldbjerg, R.; Dang, D. A.; Autrup, H. Cytotoxicity and Genotoxicity of Silver Nanoparticles in the Human Lung Cancer Cell Line, A549. *Arch. Toxicol.* **2011**, *85*, 743–750.
30. Chithrani, B. D.; Chan, W. C. Elucidating the Mechanism of Cellular Uptake and Removal of Protein-Coated Gold Nanoparticles of Different Sizes and Shapes. *Nano Lett* **2007**, *7*, 1542–1550.
31. Rejman, J.; Oberle, V.; Zuhorn, I. S.; Hoekstra, D. Size-Dependent Internalization of Particles *Via* the Pathways of Clathrin- and Caveolae-Mediated Endocytosis. *Biochem. J.* **2004**, *377*, 159–169.
32. Gu, J.; Huang, K.; Zhu, X.; Li, Y.; Wei, J.; Zhao, W.; Liu, C.; Shi, J. Sub-150 Nm Mesoporous Silica Nanoparticles with Tunable Pore Sizes and Well-Ordered Mesostructure for Protein Encapsulation. *J. Colloid Interface Sci.* **2013**, *407*, 236–242.
33. Treuel, L.; Jiang, X.; Nienhaus, G. U. New Views on Cellular Uptake and Trafficking of Manufactured Nanoparticles. *J. R. Soc., Interface* **2013**, *10*, 20120939.
34. Wang, H.; Wu, L.; Reinhard, B. M. Scavenger Receptor Mediated Endocytosis of Silver Nanoparticles into J774a.1 Macrophages Is Heterogeneous. *ACS Nano* **2012**, *6*, 7122–7132.
35. Park, E. J.; Yi, J.; Kim, Y.; Choi, K.; Park, K. Silver Nanoparticles Induce Cytotoxicity by a Trojan-Horse Type Mechanism. *Toxicol. In Vitro* **2010**, *24*, 872–878.
36. Kim, S.; Choi, J. E.; Choi, J.; Chung, K. H.; Park, K.; Yi, J.; Ryu, D. Y. Oxidative Stress-Dependent Toxicity of Silver Nanoparticles in Human Hepatoma Cells. *Toxicol. In Vitro* **2009**, *23*, 1076–1084.
37. Manza, L. L.; Stamer, S. L.; Ham, A. J.; Codreanu, S. G.; Liebler, D. C. Sample Preparation and Digestion for Proteomic Analyses Using Spin Filters. *Proteomics* **2005**, *5*, 1742–1745.
38. Wisniewski, J. R.; Zougman, A.; Nagaraj, N.; Mann, M. Universal Sample Preparation Method for Proteome Analysis. *Nat. Methods* **2009**, *6*, 359–362.
39. Kall, L.; Canterbury, J. D.; Weston, J.; Noble, W. S.; MacCoss, M. J. Semi-Supervised Learning for Peptide Identification from Shotgun Proteomics Datasets. *Nat. Methods* **2007**, *4*, 923–925.
40. Benjamini, Y.; Hochberg, Y. Controlling the False Discovery Rate: A Practical and Powerful Approach to Multiple Testing. *J. R. Stat. Soc., B* **1995**, *57*, 289–300.
41. Neuhoff, V.; Stamm, R.; Eibl, H. Clear Background and Highly Sensitive Protein Staining with Coomassie Blue Dyes in Polyacrylamide Gels: A Systematic Analysis. *Electrophoresis* **1985**, *6*, 427–448.
42. Anderson, J. P.; Williams, J. G.; Grone, D. L.; Nichols, M. G. Metal Enhancement of near-Ir Fluorescence for Molecular Biotechnology Applications. In *Reviews in Fluorescence 2009*; Geddes, C. D., Ed.; Springer: New York, 2011; pp 1−22.
43. Aiboushev, A. V.; Astafiev, A. A.; Lozovik, Y. E.; Merkulova, S. P.; Nadtochenko, V. A.; Sarkisov, O. M.; Willander, M. Enhanced Luminescence and Two-Photon Absorption of Silver Nano-Clusters. *Phys. Status Solidi C* **2009**, *6*, S162–S166.